Structural Stability and Electronic Properties of Boron Phosphide Nanotubes: A Density Functional Theory Perspective

Dolores García-Toral [1,*], Raúl Mendoza-Báez [2], Ernesto Chigo-Anota [1], Antonio Flores-Riveros [3], Víctor M. Vázquez-Báez [4], Gregorio Hernández Cocoletzi [3] and Juan Francisco Rivas-Silva [3]

[1] Facultad de Ingeniería Química, Benemérita Universidad Autónoma de Puebla, Av. San Claudio y 18 Sur S/N, San Manuel, Puebla 72570, Mexico; ernesto.chigo@correo.buap.mx

[2] Departamento de Química, Centro de Investigación y de Estudios Avanzados del IPN (Cinvestav), Av. IPN 2508, Col. San Pedro Zacatenco, Mexico City 07360, Mexico; raul.mendoza@cinvestav.mx

[3] Instituto de Física, Benemérita Universidad Autónoma de Puebla, Av. San Claudio y Blvd. 18 Sur, Col. San Manuel, Puebla 72570, Mexico; flores@ifuap.buap.mx (A.F.-R.); cocoletz@ifuap.buap.mx (G.H.C.); rivas@ifuap.buap.mx (J.F.R.-S.)

[4] Facultad de Ingeniería, Benemérita Universidad Autónoma de Puebla, Puebla 72570, Mexico; manuel.vazquez@correo.buap.mx

* Correspondence: dolores@ifuap.buap.mx

Abstract: Based on the Density Functional Theory (DFT) calculations, we analyze the structural and electronic properties of boron phosphide nanotubes (BPNTs) as functions of chirality. The DFT calculations are performed using the M06-2X method in conjunction with the 6-31G(d) divided valence basis set. All nanostructures, $(n,0)$ BPNT (n = 5–8, 10, 12, 14) and (n,n) BPNT (n = 3–11), were optimized minimizing the total energy, assuming a non-magnetic nature and a total charge neutrality. Results show that the BPNT diameter size increases linearly with the chiral index "n" for both chiralities. According to the global molecular descriptors, the (3,3) BPNT is the most stable structure provided that it shows the largest global hardness value. The low chirality (5,0) BPNT has a strong electrophilic character, and it is the most conductive system due to the small |HOMO-LUMO| energy gap. The chemical potential and electrophilicity index in the zigzag-type BPNTs show remarkable chirality-dependent behavior. The increase in diameter/chirality causes a gradual decrease in the |HOMO-LUMO| energy gap for the zigzag BPNTs; however, in the armchair-type BPNTs, a phase transition is generated from a semiconductor to a conductor system. Therefore, the nanostructures investigated in this work may be suggested for both electrical and biophysical applications.

Keywords: boron phosphide nanotubes; density functional theory; chirality; electronic properties; structural properties

1. Introduction

Since the discovery of the single-walled carbon nanotubes (SWCNT) in 1991 [1], numerous investigations have been conducted on their structural, chemical, physical, mechanical and electronic properties, which have proven to be extraordinary for certain applications. There exists an increased interest in fabricating novel inorganic analogues to CNTs made up of group III and V elements of the periodic table (groups neighboring the carbon group), such as nitrides and phosphides of boron, aluminum, gallium and indium (BN, AlN, GaN, InN, BP, AlP, GaP and InP, respectively). Among them, boron nitride nanotubes (BNNTs), as predicted in 1994 [2] and synthesized in 1995 [3], have been quite attractive and extensively investigated. Despite their structural similarity, CNT electronic properties show a strong dependence on the chirality [4–7], while the properties of BNNTs with large diameters remain almost constant [2,8], which in turn indicate chirality independence.

The boron composed nanotubes have been more studied than those of phosphorus. Although BPNTs have not been synthesized yet, theoretical research during the last decade suggests that BPNTs may be good adsorbent materials for some molecules of environmental, industrial, pharmaceutical and catalytic interest, such as peroxide, phenol, imidazole, thiazole, carbon monoxide and even some anions such as cyanates and thiocyanates [9–15]. Studies reveal that the band gap of BPNTs is similar to that of their silicon carbide analogs (SiCNTs) [16,17]. Furthermore, BPNTs doped with carbon, germanium, gallium, silicon and palladium atoms show a drastic change in their electronic properties as compared to the pristine state [10,17–23]. However, not much information is available about investigations focused on the dependence of the structural and electronic properties of BP nanotubes as a function of their diameter/chirality. For example, Srivastava et al. [24] describe that the value of the band gap of the zigzag-type BPNTs (*n*,0) (*n* = 4–15) ranges from a metallic to a semiconductor behavior, while Azizi et al. [25] show values corresponding to semiconductor for both armchair- (*n*,*n*) and zigzag-type (*n*,0) BPNTs.

The interest of this work is to study the structural and electronic properties of armchair- (*n*,*n*) (*n* = 3–11) and zigzag-type (*n*,0) (*n* = 5–8,10,12,14) BPNTs as functions of chirality. The nanostructures were optimized and verified by calculating the vibrational frequencies. Based on the DFT, the reactivity and chemical stability of the BPNTs are studied through cohesion energy (E_{coh}) and global molecular descriptors such as chemical potential (μ), global hardness (η), electrophilicity index (ω), energy gap (E_g), ionization potential (I) and electronic affinity (A).

2. Materials and Methods

Boron phosphide nanotube structural and electronic properties are investigated using first principles total energy calculations within the Density Functional Theory. The BPNT dangling bonds were passivated with hydrogen atoms to carry out a finite molecular study, that is, each nanotube length was limited through covalent bonds with hydrogen atoms at their ends. The number of atoms of each chemical species (H, B and P) that make up each nanotube is proportional to the chirality index (*n*). In the case of the armchair-type (*n*,*n*) BPNTs, $H = 4n$ and $B = P = 12n$, while for the zigzag-type (*n*,0) BPNTs, $H = 2n$ and $B = P = 7n$. Calculations were performed to determine the geometric optimization, the energy of the frontier molecular orbitals, HOMO and LUMO, dipole moment and the total energy. Studies account for the gas phase within the M06-2X/6-31G(*d*) approach implemented in the Gaussian 16 code [26]. The M06-2X functional is suitable to be applied in medium-sized systems [27]. Furthermore, results show that the M06-2X functional is suitable for unraveling non-covalent interactions, which allows more reliable results for later functionalization studies [28,29].

The stabilized nanotubes showed a singlet multiplicity ($M = 1$) with a neutral charge state ($Q = 0$). Vibrational frequency calculations were performed to verify that the structures relax with local minima. The reactivity of the systems was determined using global quantum molecular descriptors such as chemical potential (μ), global hardness (η) and electrophilicity index (ω), obtained from the HOMO and LUMO energies through the quantities obtained using Koopmans' theorem [30]:

$$I = -E_{HOMO}, \tag{1}$$

$$A = -E_{LUMO}, \tag{2}$$

where I is the ionization potential and A is the electron affinity. This is true for density functionals that correctly describe the derivative discontinuity at the integer particle numbers. Since M06-2X includes 54% of the HF exchange, we expect this functional to yield accurate estimates. Therefore, the chemical potential (μ) and global hardness (η) can be calculated with the following equations:

$$\mu = \left(\frac{\partial E}{\partial N}\right)_{\nu(r)} = -\frac{I + A}{2} \tag{3}$$

$$\eta = \left(\frac{\partial^2 E}{\partial N^2}\right)_{\nu(r)} = \frac{I - A}{2} \tag{4}$$

where E is the total energy, N is the number of electrons and $\nu(r)$ is the external potential of the system [31]. The global electrophilicity index (ω) is described by Parr [32], which uses the electronic chemical potential and is given by:

$$\omega = \frac{\mu^2}{2\eta} \tag{5}$$

This descriptor measures the tendency of the chemical species to accept electrons. Small values of ω indicate that the chemical species behaves as an electron donor (nucleophile), while high values of ω characterize the electron acceptor (electrophile).

The stability of all the nanotubes was validated by calculating the cohesion energy, which is expressed as:

$$E_{coh} = \frac{E_{BPNT} - \left(n_B E_{Boron} + n_P E_{Phosp} + n_H E_{Hydro}\right)}{n_B + n_P + n_H} \tag{6}$$

where E_{BPNT} is the total energy of the nanotube, while n_B, n_P, n_H, E_{Boron}, E_{Phosp} and E_{Hydro} represent the number of atoms and total energies of the isolated boron, phosphorus and hydrogen atoms, respectively. The E_{coh} is expressed in $eV/atom$. A stable geometry will be characterized by a negative cohesion energy.

Solvation energies (E_{Solv}) of each BPNT were obtained based on the total energy of the optimized nanotube in vacuum (E_{BPNT}) and water ($E_{BPNT-CPCM}$) (via Conductor-like Polarizable Continuum Model), as indicated by the following equation:

$$E_{Solv} = E_{BPNT-CPCM} - E_{BPNT} \tag{7}$$

The more negative the E_{Solv} value is, the greater the degree of solubility of the system is.

3. Results and Discussion

### 3.1. Structural Properties

The diameter size trend with respect to the chirality in each nanotube is shown in Figure 1. It is evident that for both armchair- and zigzag-type nanotubes, as the chiral index increases, the diameter increases almost linearly, whose coefficients of determination (termed as R2) are 0.9984 and 0.9996 for the (*n*,*n*) BPNT and (*n*,0) BPNT, respectively. These R2 values indicate a very good linear fit since values are close to unity. Table 1 shows in detail the diameter size corresponding to each nanotube.

Table 1. Diameter length (Å) for the geometrically optimized armchair- (*n*,*n*) and zigzag-type (*n*,0) BP nanotubes as calculated with the M06-2X/6-31G(*d*) method.

Chirality/Index	*n* = 3	4	5	6	7	8	9	10	11	12	14
(*n*,0)	-	-	5.56	6.46	7.43	8.44	-	10.42	-	12.55	14.40
(*n*, *n*)	5.19	6.85	8.15	9.99	12.11	13.91	15.55	17.38	19.31	-	-

The axial length of each nanotube shows no considerable variation with respect to the chirality, with an average value of 19.94 Å and 17.98 Å for armchair- and zigzag-type nanotubes, respectively. Tables 2 and 3 summarize the relaxed bond lengths and angles. In both cases, the B-P bond length decreases as the chirality index increases. The average length of the B-P bond for both chiralities is ~1.88 Å. In addition, the boron–hydrogen bond length is shorter than that of the phosphorus–hydrogen bond ($B - H < P - H$), because

of the electronegativity difference in the B-H, which is greater than in the P-H, inducing a more strengthened bond. The average value of the angle formed by the P-B-P atoms is 120.08° and 120.45° for armchair- and zigzag-type BPNTs, respectively. The angles of the H-P-B and H-B-P bonds at the ends of armchair and zigzag nanotubes increase slightly with increasing chirality. This small increase occurs because of chirality increase, as there is a higher density of hydrogen atoms at the end of the tube, causing a repulsion effect between them, which in turn generates an increase in the formed angle. The cohesion energy values are reported in Table 4 (armchair type) and Table 5 (zigzag type). Negative values were obtained for each nanotube, with an average value of −2.96 eV/atom for armchair-type and −2.95 eV/atom for zigzag-type BPNTs, indicating that they are all stable structures. These values suggest that pristine BPNTs are less stable than CNTs and BNNTs, since the latter have cohesion energies of −8.72 and −7.27 eV, respectively [33]. For both types of chirality, the cohesion energy decreases as the chiral index (n) increases, indicating that the greater the diameter is, the better the stability of the system is. However, the decrease in E_{coh} is very small, since the energy difference between the maximum and the minimum value is only 0.13 eV/atom, both in the armchair- and zigzag-type. Vibrational frequency calculations showed that all nanotubes have non-imaginary frequencies.
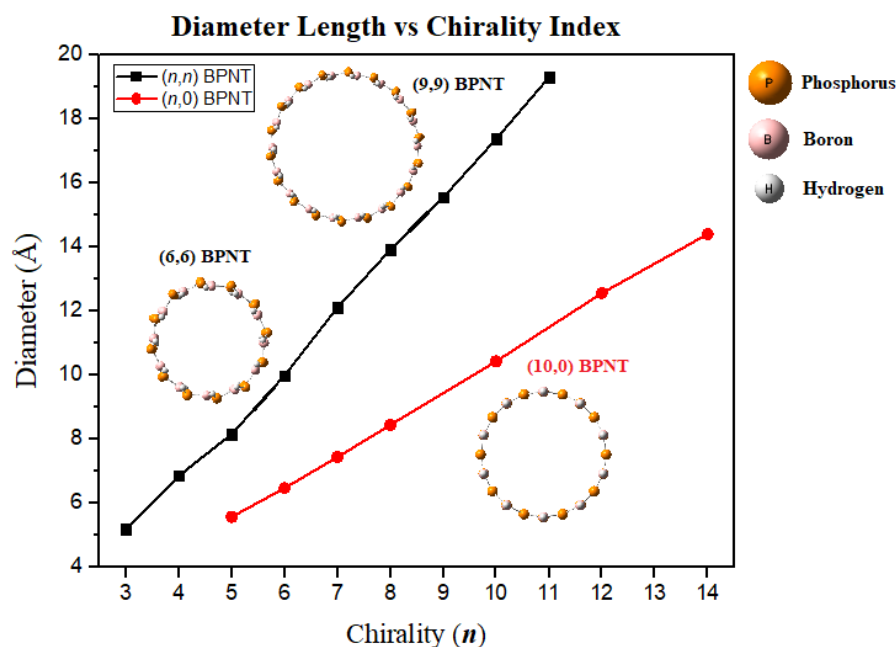
Figure 1. Diameter length (Å) as a function of chiral index (n). The black line corresponds to the armchair-type nanotubes, while the red line to the zigzag type. Atom colors: orange—phosphorus; pink—boron; white—hydrogen.

Table 2. Bond length (Å) and bond angle (°) values of armchair-type (n,n) BP nanotubes (where n = 3–11) optimized via DFT/M06-2X/6-31G(d).

Nanotube	Bond Lengths (Å)				Angle (°)			
Armchair	Axial Length	B-P	P-H	B-H	P-B-P	B-P-B	H-P-B	H-B-P
(3,3)	19.8894	1.9129	1.4259	1.1861	122.2794	109.5253	108.55	118.1869
(4,4)	19.9063	1.8924	1.4209	1.1859	119.2242	114.2072	109.4626	118.777
(5,5)	19.9237	1.8862	1.4187	1.1856	120.7065	115.1849	111.0487	119.6057
(6,6)	19.9376	1.8814	1.4166	1.1857	119.691	116.4117	111.9162	119.8233
(7,7)	19.9503	1.8798	1.4152	1.1856	119.6188	117.8321	112.3506	119.6171
(8,8)	19.9618	1.8771	1.4143	1.1856	119.4768	118.3511	112.997	119.7843
(9,9)	19.9708	1.8756	1.4134	1.1855	119.8691	118.3118	113.6048	119.9248
(10,10)	19.9805	1.8747	1.4127	1.1856	120.1455	118.9187	114.2501	120.085
(11,11)	19.9861	1.875	1.4122	1.1854	119.7613	119.2771	114.7068	120.1182

Table 3. Bond length (Å) and bond angle (°) values of zigzag-type (*n*,0) BP nanotubes (where *n* = 5–8, 10, 12, 14) optimized via DFT/M06-2X/6-31G(*d*).

Nanotube	Bond Lengths (Å)					Angle (°)			
Zigzag	Axial Length	B-P	P-H	B-H	P-B-P	B-P-B	H-P-B	H-B-P
(5,0)	17.8614	1.9135	1.4351	1.1861	120.8479	105.0648	101.9944	117.7055
(6,0)	17.9346	1.8995	1.4316	1.1858	121.7117	110.9808	102.8412	117.5638
(7,0)	17.9806	1.8939	1.4294	1.1856	120.3019	111.5138	104.9868	118.5491
(8,0)	17.9966	1.8851	1.4279	1.1854	120.3811	114.968	105.9255	118.8265
(10,0)	18.0259	1.8819	1.4255	1.1852	119.7837	115.6483	107.5051	119.1812
(12,0)	18.0435	1.8778	1.424	1.1848	119.8862	116.4566	108.7472	119.3955
(14,0)	18.0537	1.8775	1.4228	1.185	120.2846	118.1968	109.7213	119.513

Table 4. Optimized total energy (E_{Total}), energy of the highest occupied molecular orbital (E_{HOMO}), energy of the lowest unoccupied molecular orbital (E_{LUMO}), energies of the quantum molecular descriptors (η, μ, ω) and cohesion energy (E_{coh}) for armchair-type BPNTs. All values are given in eV units and performed via DFT/M06-2X/6-31G(*d*).

Armchair BPNT	Quantum Molecular Descriptors and E_{coh} for (*n*,*n*) BPNTs								
Descriptors	(3,3)	(4,4)	(5,5)	(6,6)	(7,7)	(8,8)	(9,9)	(10,10)	(11,11)
E_{TOTAL}	−358,734.516	−478,319.133	−597,903.132	−717,486.631	−837,069.831	−956,652.817	−1,076,235.658	−1,195,818.389	−1,315,401.058
E_{HOMO}	−6.8995	−6.7725	−6.6888	−6.6428	−6.6145	−6.5971	−6.5857	−6.5764	−6.5712
E_{LUMO}	−5.6244	−5.7531	−5.9084	−5.9922	−6.0406	−6.0694	−6.0874	−6.0988	−6.1061
Eg Gap	1.2751	1.0195	0.7804	0.6506	0.5739	0.5277	0.4983	0.4776	0.4651
$I = -E_{HOMO}$	6.8996	6.7725	6.6888	6.6428	6.6145	6.5971	6.5857	6.5764	6.5712
$A = -E_{LUMO}$	5.6244	5.7531	5.9084	5.9922	6.0406	6.0694	6.0874	6.0988	6.1061
$\eta = (I - A)/2$	0.6376	0.5097	0.3902	0.3253	0.2870	0.2638	0.2492	0.2388	0.2326
$\mu = -(I + A)/2$	−6.2620	−6.2628	−6.2986	−6.3175	−6.3275	−6.3332	−6.3365	−6.3376	−6.3387
$\omega = \mu^2/2\eta$	30.7516	38.4741	50.8375	61.3418	69.7618	76.0120	80.5761	84.0923	86.3841
E_{coh}	−2.8618	−2.9193	−2.9494	−2.9665	−2.9772	−2.9843	−2.9892	−2.9927	−2.9954

Table 5. Optimized total energy (E_{Total}), energy of the highest occupied molecular orbital (E_{HOMO}), energy of the lowest unoccupied molecular orbital (E_{LUMO}), energies of the quantum molecular descriptors (η, μ, ω) and cohesion energy (E_{coh}) for zigzag-type BPNTs. All values are given in eV and as calculated via DFT/M06-2X/6-31G(*d*).

Zigzag BPNT	Quantum Molecular Descriptors and E_{coh} for (*n*,0) BPNTs						
Descriptors	(5,0)	(6,0)	(7,0)	(8,0)	(10,0)	(12,0)	(14,0)
E_{TOTAL}	−348,742.4988	−418,495.3783	−488,247.8623	−558,000.0492	−697,503.8110	−837,007.0566	−976,509.9845
E_{HOMO}	−6.9882	−6.9210	−7.0652	−6.8106	−6.8770	−6.7910	−6.7140
E_{LUMO}	−6.9077	−6.7092	−6.4298	−6.2049	−5.8934	−5.9500	−6.0411
Eg Gap	0.0805	0.2119	0.6354	0.6057	0.9836	0.8410	0.6729
$I = -E_{HOMO}$	6.9882	6.9210	7.0652	6.8106	6.8770	6.7910	6.7140
$A = -E_{LUMO}$	6.9077	6.7092	6.4298	6.2049	5.8934	5.9500	6.0411
$\eta = (I - A)/2$	0.0403	0.1059	0.3177	0.3029	0.4918	0.4205	0.3365
$\mu = -(I + A)/2$	−6.9480	−6.8151	−6.7475	−6.5077	−6.3852	−6.3705	−6.3776
$\omega = \mu^2/2\eta$	599.5909	219.1985	71.6547	69.9151	41.4526	48.2548	60.4427
E_{coh}	−2.8633	−2.9090	−2.9380	−2.9575	−2.9809	−2.9939	−3.0017

The calculated IR spectra of all systems are shown in Figures 2 and 3 for the armchair- and zigzag-type boron phosphide nanotubes, respectively. In both cases, a pair of sets of characteristic peaks are noted in the frequency region of >2400 cm^{-1}, corresponding to the P-H stretch vibration (2503–2521 cm^{-1}) and the B-H stretch vibration (~2725 cm^{-1}). The highest ε intensity peaks occur in the frequency range between 850–1100 cm^{-1}, again for both cases, attributed to a P-B-P stretch vibration (900–955 cm^{-1}) and to the B-H bending vibration (1031–1040 cm^{-1}). It is noted that the P-B-P stretch vibration mode is affected by a blue shift when the chiral index increases (+10 cm^{-1}/*n*, Figures 2b and 3b). The armchair- and zigzag-type BPNTs display a very similar IR spectra; however, the armchair-type nanotubes exhibit a characteristic small peak in the frequency range of 820–840 cm^{-1} corresponding to the P-H bond bending mode. This characteristic signal allows differentiating

between both chiralities. In general, the peak intensity increases with the chiral index, as induced by the number of bonds present in the structure.

(**a**)　　　　　　　　　　　　　　　　　　　　　(**b**)
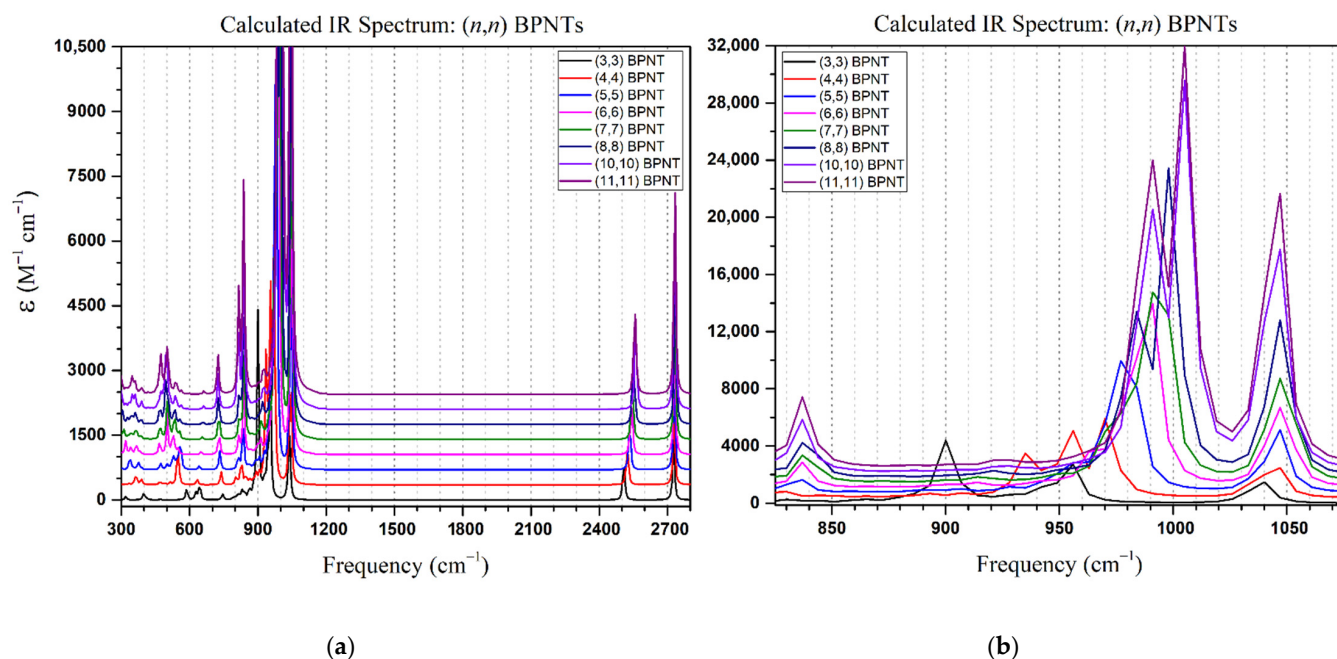
Figure 2. (**a**) Theoretical IR spectra of armchair-type BPNTs; (**b**) close-up in range from 825 cm^{-1} to 1075 cm^{-1}. The signal of the peaks was shifted by 350 ε units relative to each other.


(**a**)　　　　　　　　　　　　　　　　　　　　　(**b**)
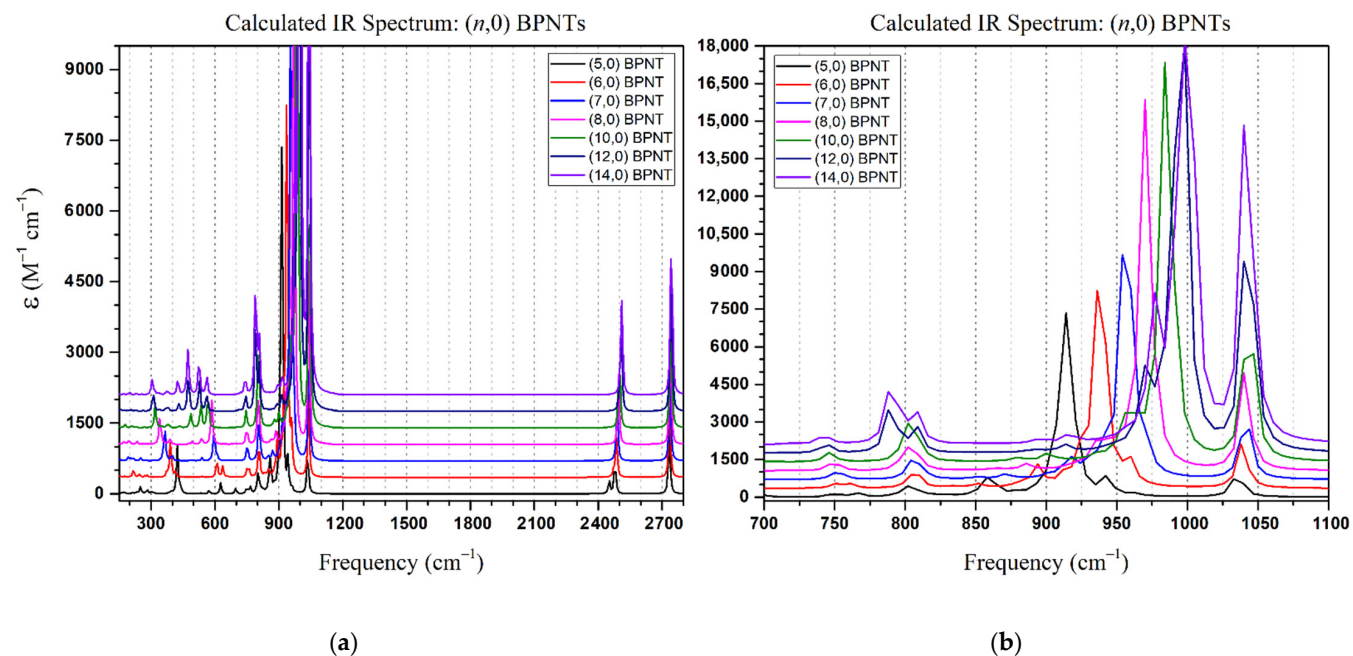
Figure 3. (**a**) Theoretical IR spectra of zigzag-type BPNTs; (**b**) close-up in range from 700 cm^{-1} to 1100 cm^{-1}. The signal of the peaks was shifted by 350 ε units relative to each other.

3.2. Electronic Properties

The highest occupied molecular orbital (HOMO) and the lowest unoccupied molecular orbital (LUMO) are discussed in this section. Figure 4 shows the |HOMO-LUMO| energy gaps as functions of the chirality as obtained in this work and compared with those obtained in the previously mentioned reports (see Introduction Section). The energy gap of

the (*n*,*n*) BPNTs decreases as the index (diameter) increases, reaching stabilization when $n \geq 10$, (10,10) BPNT. This characteristic has also been reported for BNNT and SiCNT, where starting at a certain diameter the band gap energy is chirality independent [16,24]. On the other hand, zigzag nanotubes transform from a metallic character (5,0) BPNT with 0.08 eV to semiconductor, with (10,0) BPNT being the one with a larger energy gap value (0.98 eV). Thus, low chirality zigzag BPNTs can be used in electronic and energy transport devices. It can be noted that, in the case of zigzag BPNTs, our values have a similar trend and are close to those reported by Srivastava et al. [24], particularly with those calculated by the LDA/PZ/DZP method. However, our results differ largely from those described by Azizi et al. [25] for both armchair- and zigzag-type nanotubes. Other authors have also reported the value of the energy gap for some chiralities in studies about the functionalization of boron phosphide nanotubes. Table 6 summarizes these values reported by different authors [9–12,14,15,17,18,20–22,34–37] for the nanotubes (5,0), (6,0), (7,0), (8,0) and (4,4), comparing them with the values obtained in this work. Considerable different values of molecular gap are noted for the same chirality, however, all the values reported by other authors are calculated with the B3LYP or BLYP functional. This suggests that there is an underestimation or overestimation when calculating the HOMO-LUMO gap when the functionals B3LYP/BLYP and the M06-2X are used, respectively. Another factor that could be responsible for this difference in the molecular gap is the number of atoms that make up the nanotube, that is, its molecular formula. For all the cases shown in Table 6, our models of BPNTs have a larger number of atoms and, therefore, a greater length, because chirality determines the diameter of the nanotube but not its length. This would be a great challenge to synthesize BPNTs in a controlled way, since their electronic properties would present a strong dependence on the length of the nanotube.
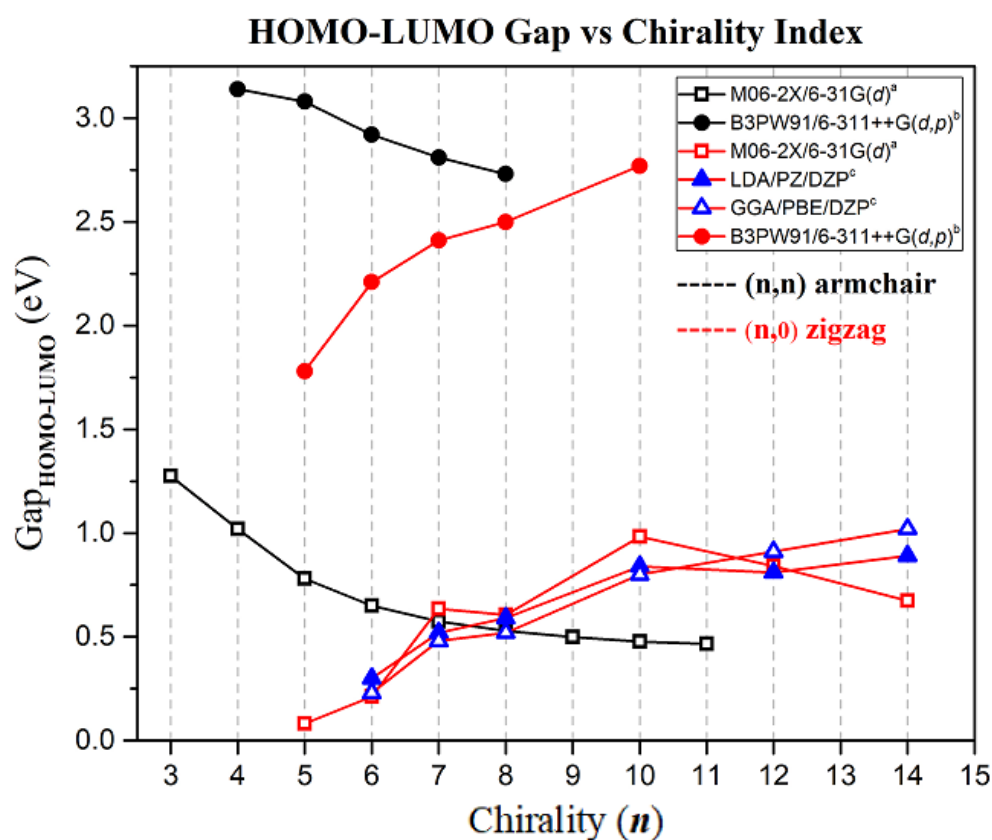
Figure 4. |HOMO-LUMO| energy gaps as functions of the chiral index (*n*) for armchair- (black line) and zigzag-type (red line) BPNTs. Comparison of values calculated in: [a] this work (unfilled squares), and in Refs; [b] [25] (filled circles) and [c] [24] (filled/unfilled triangles).

Table 6. Review of the HOMO-LUMO gap values (eV) reported in the literature for different boron phosphide nanotubes. Values calculated by this work (Gaussian16/M06-2X/6-31G(*d*)) and references.

Summary of HOMO-LUMO Gap Values and Molecular Formula Reported in the Literature				
Chirality	Software + Method	HOMO-LUMO Gap	Molecular Formula	Reference
(5,0)	GAMESS/B3LYP/6-31G(*d,p*)	1.62	$B_{27}P_{27}H_{10}$	[34]
(5,0)	Gaussian16/M06-2X/6-31G(*d*)	0.0805	$B_{35}P_{35}H_{10}$	This work
(6,0)	Gaussian03/B3LYP/6-31G(*d*)	2.27	$B_{24}P_{24}H_{12}$	[12]
(6,0)	Gaussian03/B3LYP/6-31G(*d*)	2.43	$B_{24}P_{24}H_{12}$	[18]
(6,0)	GAMESS/B3LYP/6-31G(*d*)	1.93	$B_{36}P_{36}H_{12}$	[14]
(6,0)	Gaussian98/BLYP/6-31G(*d*)	1.09	$B_{24}P_{24}H_{12}$	[35]
(6,0)	GAMESS/B3LYP/6-31G(*d*)	2.06	$B_{30}P_{30}H_{12}$	[11]
(6,0)	Gaussian98/BLYP/6-31G(*d*)	1.09	$B_{24}P_{24}H_{12}$	[17]
(6,0)	Gaussian03/B3LYP/6-31G(*d*)	2.06	$B_{30}P_{30}H_{12}$	[10]
(6,0)	Gaussian98/B3LYP/6-311G(*d,p*)	2.25	$B_{24}P_{24}H_{12}$	[36]
(6,0)	Gaussian98/B3LYP/6-31G(*d*)	2.27	$B_{24}P_{24}H_{12}$	[15]
(6,0)	Gaussian16/M06-2X/6-31G(*d*)	0.2118	$B_{42}P_{42}H_{12}$	This work
(7,0)	GAMESS/B3LYP/6-31G(*d*)	2.22	$B_{42}P_{42}H_{14}$	[14]
(7,0)	Gaussian16/M06-2X/6-31G(*d*)	0.6353	$B_{49}P_{49}H_{14}$	This work
(8,0)	Gaussian03/B3LYP/6-31G(*d*)	2.57	$B_{32}P_{32}H_{16}$	[20]
(8,0)	Gaussian16/M06-2X/6-31G(*d*)	0.6057	$B_{56}P_{56}H_{16}$	This work
(4,4)	Gaussian98/BLYP/6-31G(*d*)	1.77	$B_{28}P_{28}H_{16}$	[17]
(4,4)	Gaussian03/B3LYP/6-31G(*d*)	2.95	$B_{28}P_{28}H_{16}$	[9]
(4,4)	Gaussian98/BLYP/6-31G(*d*)	1.77	$B_{28}P_{28}H_{16}$	[35]
(4,4)	GAMESS/B3LYP/6-31G(*d*)	2.95	$B_{28}P_{28}H_{16}$	[14]
(4,4)	Gaussian03/BLYP/6-31G(*d*)	1.75	$B_{28}P_{28}H_{16}$	[22]
(4,4)	Gaussian03/B3LYP/6-31G(*d*)	2.95	$B_{28}P_{28}H_{16}$	[22]
(4,4)	Gaussian03/B3LYP/6-31G(*d*)	2.95	$B_{28}P_{28}H_{16}$	[21]
(4,4)	Gaussian03/B3LYP/6-31G(*d*)	2.95	$B_{32}P_{32}H_{16}$	[37]
(4,4)	Gaussian16/M06-2X/6-31G(*d*)	1.0194	$B_{48}P_{48}H_{16}$	This work

The distribution of the HOMO and LUMO orbitals through the nanotubes are graphically depicted in Figures 5 and 6 for the armchair and zigzag BPNTs, respectively. It is evident that the HOMO orbital is uniformly distributed throughout the entire nanotube in the armchair type, however, different features display the zigzag type, since this is concentrated at one end of the nanotube. The LUMO orbital, in the zigzag-type BPNTs, is uniformly distributed until chirality (8,0). At larger index, this is concentrated at one of the extremes. In the armchair-type BPNTs, analogous to HOMO, the LUMO is distributed throughout the entire nanotube.
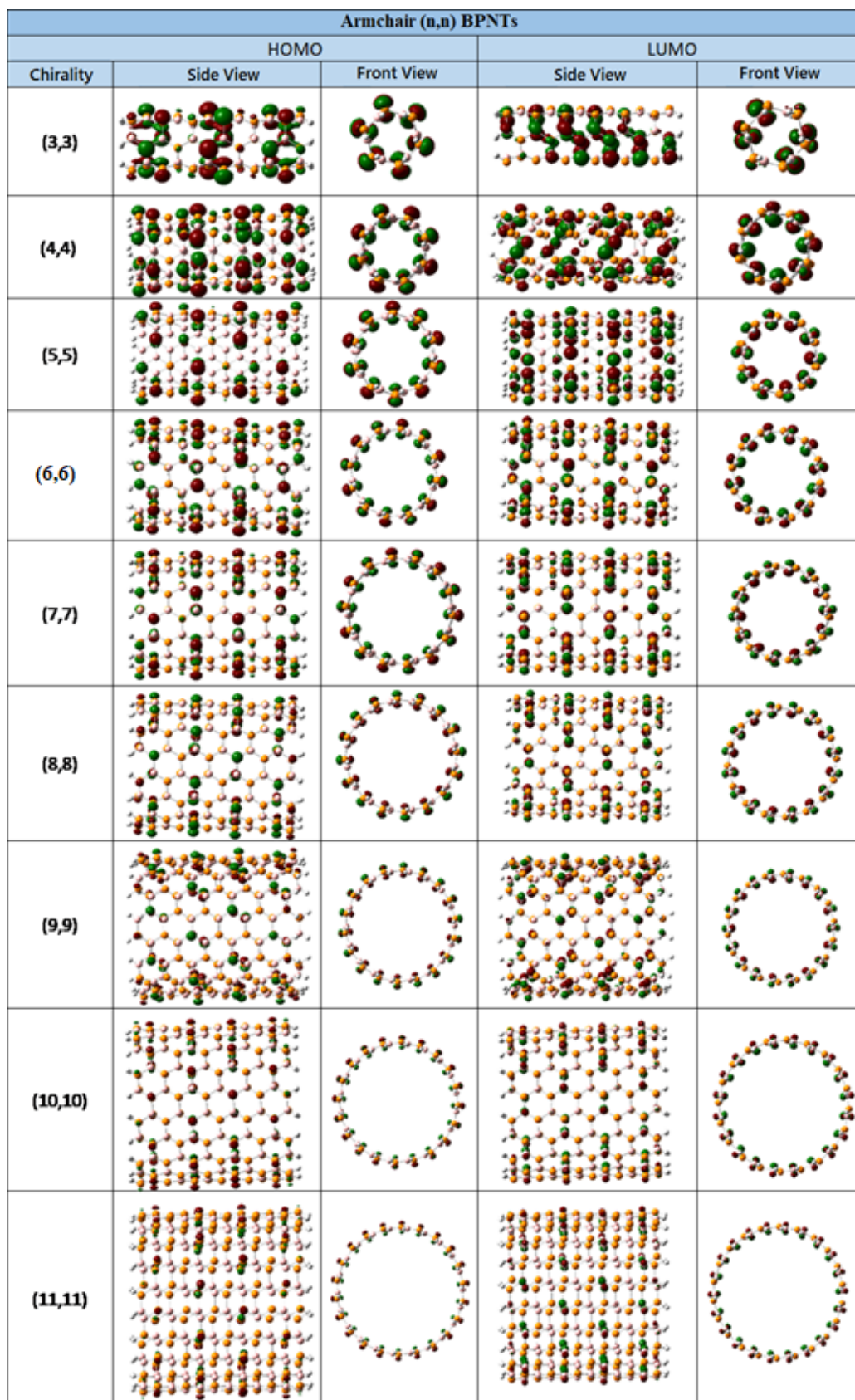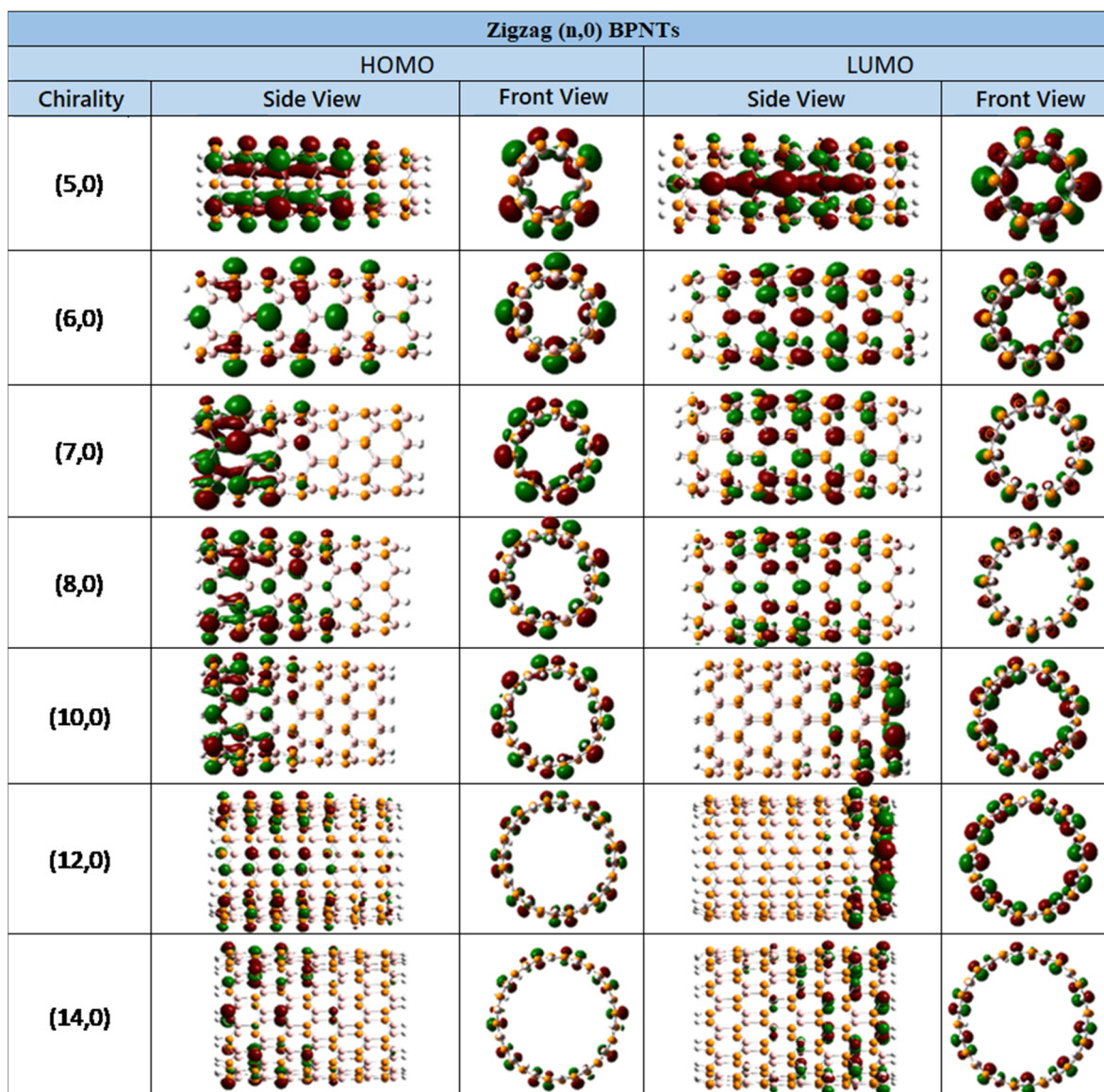
Figure 5. Spatial distribution of the HOMO and LUMO orbitals through the armchair-type BP nanotubes. Atom colors: orange—phosphorus; pink—boron; white—hydrogen.

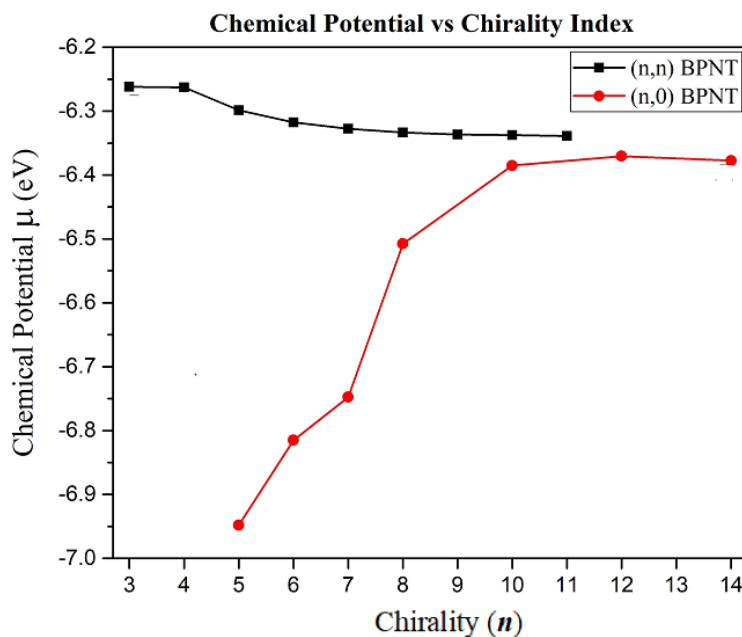| Zigzag (n,0) BPNTs				
	HOMO		LUMO	
Chirality	Side View	Front View	Side View	Front View
(5,0)				
(6,0)				
(7,0)				
(8,0)				
(10,0)				
(12,0)				
(14,0)				

Figure 6. Spatial distribution of the HOMO and LUMO orbitals through the zigzag-type BP nanotubes. Atom colors: orange—phosphorus; pink—boron; white—hydrogen.

The reactivity and chemical stability of the nanotubes was measured through global quantum molecular descriptors such as chemical potential (μ), global hardness (η) and electrophilicity index (ω), energy gap (E_g), ionization potential (I) and electronic affinity (A), as summarized in Tables 4 and 5. These parameters have been widely used for many years in computational chemistry studies [38–41] and, recently, to study the functionalization and stability of some III-V nanotubes [42–46]. The global hardness represents the system resistance to a charge transfer, that is, high values of η indicate greater electronic stability. Thus, the electronic stability of the armchair-type BPNTs decreases as chirality increases, with (3,3) BPNT being the most electronically stable system (see Figure 7). The zigzag-type BPNTs exhibit an arbitrary variation in the global hardness with respect to the chirality, showing a maximum energy value of ~0.492 eV in the (10,0) BPNT. In addition, the zigzag nanotubes display the highest (most negative) μ values and these decrease with increasing chirality, so that the zigzag BPNTs with the highest chirality are the least chemically reactive, since the chemical potential is a property that characterizes the tendency of electrons to escape from a system in equilibrium. No significant variation in the value of μ of the armchair-type BPNTs, -6.34 eV $< \mu < -6.26$ eV, is found, indicating chirality independence

(see Figure 8). However, the chemical potential of both chiralities tend to converge towards the same value, i.e., $\mu = -6.36 \, \text{eV} \pm 0.37\%$ for $n \geq 10$. Comparing the global hardness and chemical potential values of boron phosphide nanotubes with their most studied structural analogues, CNTs and BNNTs, it is noted that BPNTs show η values in a range very close to that of CNTs, however, this later structure is much smaller than those reported for the BNNTs. Moreover, in the case of the chemical potential, μ, the BPNT values are similar to those of the BNNTs, being much smaller than those reported for CNTs [46–48]. Therefore, we can establish that $\eta_{CNTs} \cong \eta_{BPNTs} \ll \eta_{BNNTs}$ and $|\mu_{CNTs}| < |\mu_{BPNTs}| \cong |\mu_{BNNTs}|$.
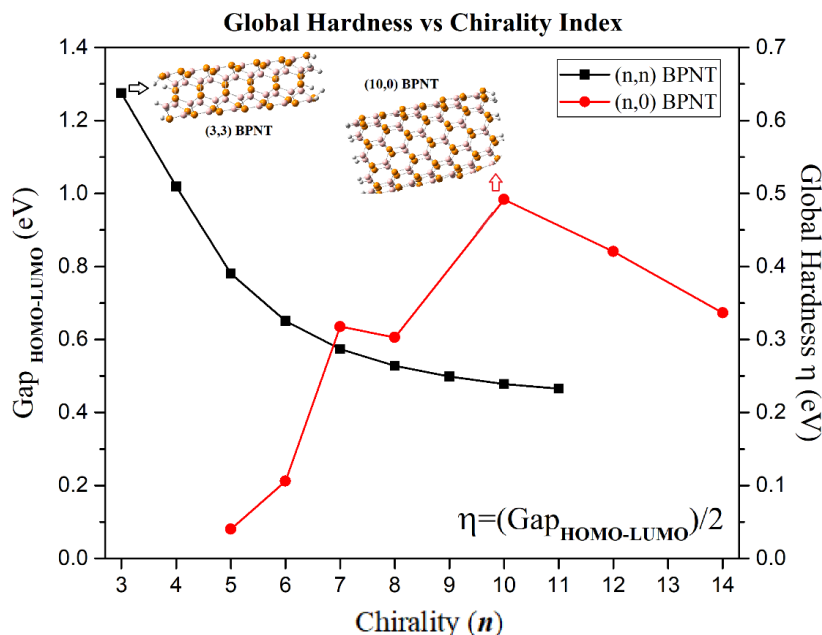

Figure 7. |HOMO-LUMO| gap and global hardness as functions of the chiral index for armchair-type (black line) and zigzag-type (red line) BPNTs. Inset: equation of the relationship between |HOMO-LUMO| gap and global hardness (bottom); (3,3) and (10,0) BPNTs (top).

Figure 8. Chemical potential behavior as a function of the chiral index for armchair-type (black line) and zigzag-type (red line) BPNTs.

Regarding the electrophilicity index, the (5,0) BPNT exhibits a large value provided that ω (599.59 eV) is large. However, the electrophilic character of the zigzag BPNTs drops abruptly with increasing chirality, while in the armchair type, this parameter increases gradually (see Figure 9). The ionization potential (I) measures the tendency to yield electrons, while electron affinity (A) measures the tendency to accept electrons. Thus, high ionization potential values indicate that large energy is required to yield electrons from the HOMO orbital, while large values of electron affinity indicate high electron accepting capacity. Both the armchair- and the zigzag-type chiralities exhibit large energy values of I and A, therefore, BPNTs are systems that easily accept electrons. This justifies their great electrophilic character, as indicated by the ω index.

**Electrophilicity Index vs Chirality Index**
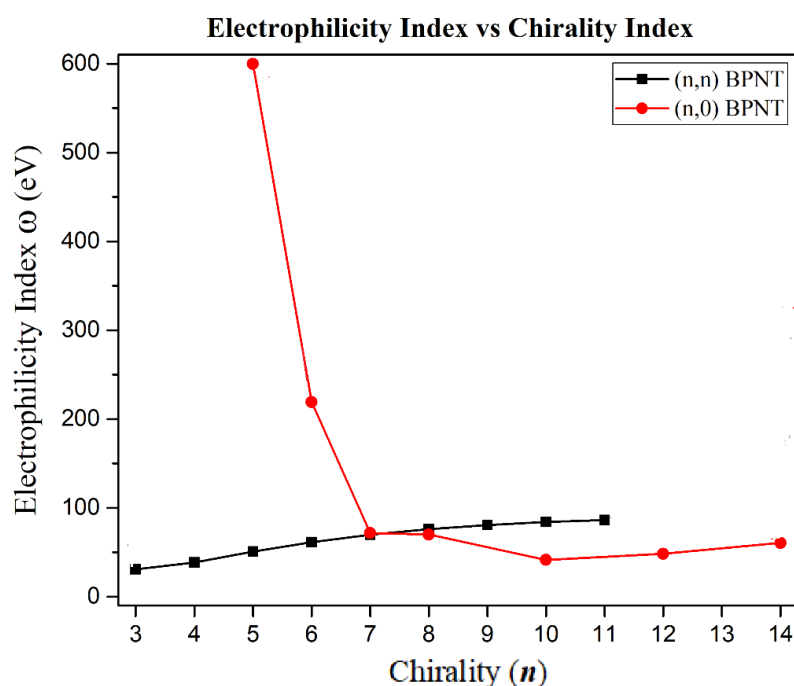
Figure 9. Electrophilicity index behavior as a function of the chiral index for armchair-type (black line) and zigzag-type (red line) BPNTs.

The dipole moment $\vec{\mu}_D$ is a quantitative measure of the dipole moment magnitude and allows differentiating between polar and non-polar molecules. It is considered to a certain extent an index of reactivity, which is very important to define some biological properties [49]. The dipole moment of a polyatomic system is the vector sum of the bond dipoles. Our results show that the (*n*,*n*) BPNTs exhibit nearly zero dipole moment values (i.e., non-polar systems), as induced by the structural symmetry of the armchair-type nanotubes (see Figure 10). Nearly-zero polarity is independent of the type of atoms that make up the nanotube, since other nanotubes such as GaNNT, BNNT and AlNNT also display null dipole moment values of armchair-type chirality [43,50]. On the other hand, zigzag-type nanotubes are polar structures, with the (14,0) BPNT being the one with the largest value $\vec{\mu}_D = 2.32\ D$, although with no dependence of polarity ($\vec{\mu}_D$) on the chiral index (*n*). This suggests that zigzag-type boron phosphide nanotubes are more soluble than armchair-type structures in polar solvents such as water, which in turn indicates that they are suitable for applications in biological systems. This characteristic of zigzag-type nanotubes of having a higher dipole moment, and therefore greater solubility, compared to armchair type, has also been reported for BNNTs [51,52]. These results make it clear that the zigzag-type nanotubes have a higher degree of solubility, since polarity is a key property for high solubility. We can validate this through the solvation energy values calculated using Equation (7). The results show that, in general, the solvation energy in the zigzag type is higher (more negative) than in armchair nanotubes, as expected. It may be thought

that Figure 11 contradicts this last assertion since, for example, the armchair-type (11,11) BPNT has higher E_{Solv} values than most of the zigzag-type nanotubes. However, this is not an appropriate comparison, since the (11,11) BPNT contains a much larger number of atoms that promotes intermolecular interactions which in turn favors solvation. Then, it is necessary to compare the E_{Solv} values between nanotubes with a similar number of atoms and having almost the same diameters, for example the (5,5) BPNT (−12.08 kcal/mol) vs. (8,0) BPNT (−17.27 kcal/mol) or the (6,6) BPNT (−13.49 kcal/mol) vs. (10,0) BPNT (−19.83 kcal/mol). There are several recent investigations that show the important role that the dipole moment plays on the solubility of some pristine and/or functionalized nanotubes [51–56].
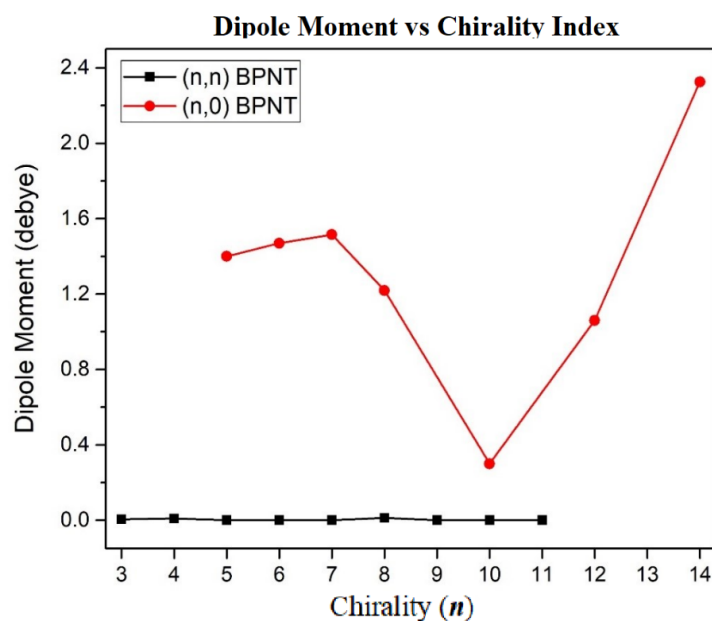
Figure 10. Dipole moment behavior as a function of the chiral index for armchair-type (black line) and zigzag-type (red line) BPNTs.
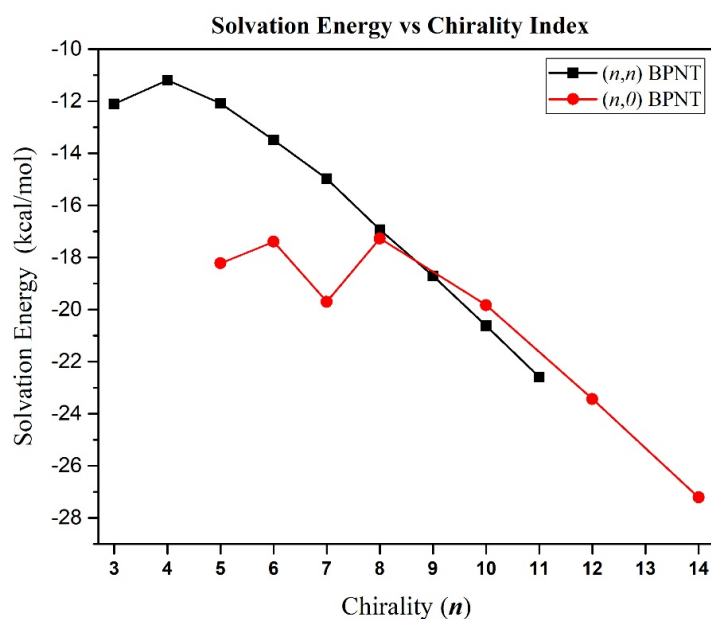
Figure 11. Solvation energy as a function of the chiral index for the armchair-type (black line) and zigzag-type (red line) BPNTs. Values were calculated using the Conductor-like Polarizable Continuum Model (CPCM), as implemented in the software package Gaussian16.

4. Conclusions

In this study, the structural and electronic properties of boron phosphide nanotubes in the zigzag and armchair chiralities were investigated. The study was conducted under the Density Functional Theory approach with the M06-2X/6-31G(*d*) method. The total energy minimization, assuming a non-magnetic nature and a total charge neutrality, yielded the ground state of all nanostructures, (*n*,0) BPNT (*n* = 5–8, 10, 12, 14) and (*n*,*n*) BPNT (*n* = 3–11). In both chiralities, results indicate that the BPNT diameter grows linearly with the chiral index (*n*). Global molecular descriptors establish that (3,3) BPNT is the most stable nanotube because it has the largest global hardness value. The (5,0) BPNT has a strong electrophilic character, acting as an excellent electron acceptor. The chemical potential and the electrophilicity index in the zigzag-type BPNTs show remarkable chirality-dependent behavior. Based on the characteristic behavior of the |HOMO-LUMO| energy gap, the zigzag-type BPNTs transform from metallic to semiconductor as their chirality increases. In contrast, the armchair-type nanotubes show a semiconductor behavior with the energy gap decreasing gradually with the increase in the chiral index. Finally, in this study of nanotubes as finite molecules, it is observed that armchair BPNTs are non-polar systems, unlike the remarkable polar behavior of zigzag-type BPNTs regardless of chirality. In general, studying the variation in the structural and electronic properties of BPNTs allows proposing these systems for possible applications. Therefore, the set of nanotubes studied in this work may be proposed for both electrical and biophysical applications.

Author Contributions: Conceptualization, D.G.-T. and R.M.-B.; methodology, J.F.R.-S.; software, E.C.-A.; validation, D.G.-T. and J.F.R.-S.; formal analysis, G.H.C.; investigation, V.M.V.-B.; resources, V.M.V.-B.; data curation, A.F.-R.; writing—original draft preparation, J.F.R.-S.; writing—review and editing, R.M.-B.; visualization, V.M.V.-B.; supervision, D.G.-T.; project administration, E.C.-A.; funding acquisition, V.M.V.-B. All authors have read and agreed to the published version of the manuscript.

Institutional Review Board Statement: Not applicable.

Informed Consent Statement: Not applicable.

Data Availability Statement: Not applicable.

Conflicts of Interest: The authors declare no conflict of interest. On behalf of all authors, the corresponding author states that there is no conflict of interest.

References

1. Iijima, S. Helical microtubules of graphitic carbon. *Nature* **1991**, *354*, 56–58. [CrossRef]
2. Rubio, A.; Corkill, J.L.; Cohen, M.L. Theory of graphitic boron nitride nanotubes. *Phys. Rev. B Condens. Matter* **1994**, *49*, 5081–5084. [CrossRef] [PubMed]
3. Chopra, N.G.; Luyken, R.J.; Cherrey, K.; Crespi, V.H.; Cohen, M.L.; Louie, S.G.; Zettl, A. Boron Nitride Nanotubes. *Science* **1995**, *269*, 966–967. [CrossRef] [PubMed]
4. Odom, T.W.; Huang, J.-L.; Kim, P.; Lieber, C.M. Structure and Electronic Properties of Carbon Nanotubes. *J. Phys. Chem. B.* **2000**, *104*, 2794–2809. [CrossRef]
5. Sfeir, M.Y. Optical Spectroscopy of Individual Single-Walled Carbon Nanotubes of Defined Chiral Structure. *Science* **2006**, *312*, 554–556. [CrossRef] [PubMed]
6. Marana, N.L.; Albuquerque, A.R.; La Porta, F.A.; Longo, E.; Sambrano, J.R. Periodic density functional theory study of structural and electronic properties of single-walled zinc oxide and carbon nanotubes. *J. Solid State Chem.* **2016**, *237*, 36–47. [CrossRef]
7. Dass, D.; Vaid, R. Chirality dependence of electronic band structure and density of states in single-walled carbon nanotubes. *Afr. Rev. Phys.* **2018**, *12*, 104–113.
8. Blase, X.; Rubio, A.; Louie, S.G.; Cohen, M.L. Stability and Band Gap Constancy of Boron Nitride Nanotubes. *Europhys. Lett. (EPL)* **1994**, *28*, 335–340. [CrossRef]
9. Baei, M.T.; Moradi, A.V.; Torabi, P.; Moghimi, M. Adsorption properties of H_2O_2 trapped inside a boron phosphide nanotube. *Monatsh. Chem.* **2011**, *143*, 37–41. [CrossRef]

10. Peyghan, A.A.; Baei, M.T.; Moghimi, M.; Hashemian, S. Theoretical Study of Phenol Adsorption on Pristine, Ga-Doped, and Pd-Decorated (6,0) Zigzag Single-Walled Boron Phosphide Nanotubes. *J. Clust. Sci.* **2012**, *24*, 49–60. [CrossRef]

11. Sayyad-Alangi, S.Z.; Hashemian, S.; Baei, M.T. Covalent Functionalization of Pristine and Ga-Doped Boron Phosphide Nanotubes with Imidazole. *Phosphorus Sulfur Silicon Relat. Elem.* **2014**, *189*, 453–464. [CrossRef]

12. Sayyad-Alangi, S.Z.; Baei, M.T.; Hashemian, S. Adsorption and electronic structure study of thiazole on the (6,0)zigzagsingle-walled boron phosphide nanotube. *J. Sulphur Chem.* **2013**, *34*, 407–420. [CrossRef]

13. Beheshtian, J.; Baei, M.T.; Peyghan, A.A. Theoretical study of CO adsorption on the surface of BN, AlN, BP and AlP nanotubes. *Surf. Sci.* **2012**, *606*, 981–985. [CrossRef]

14. Kanani, Y.; Baei, M.T.; Moradi, A.V.; Soltani, A. Adsorption mechanism of single OCN− and SCN− upon single-walled BP nanotubes. *Phys. E Low Dimens. Syst. Nanostruct.* **2014**, *59*, 66–74. [CrossRef]

15. Soltani, A.; Taghartapeh, M.R.; Mighani, H.; Pahlevani, A.A.; Mashkoor, R. A first-principles study of the SCN− chemisorption on the surface of AlN, AlP, and BP nanotubes. *Appl. Surf. Sci.* **2012**, *259*, 637–642. [CrossRef]

16. Wu, I.J.; Guo, G.Y. Optical properties of SiC nanotubes: An ab initio study. *Phys. Rev. B Condens. Matter* **2007**, *76*, 035343. [CrossRef]

17. Mirzaei, M. Carbon doped boron phosphide nanotubes: A computational study. *J. Mol. Model.* **2010**, *17*, 89–96. [CrossRef]

18. Esrafili, M.D. Carbon-Doped (6,0) Single-Walled Boron-Phosphide Nanotubes: A DFT Investigation of Electronic Structure, Surface Electrostatic Potential and QTAIM Analysis. *Fuller. Nanotub. Carbon Nanostruct.* **2014**, *23*, 142–147. [CrossRef]

19. Baei, M.T.; Moghimi, M.; Torabi, P.; Moradi, A.V. The Ge-doped (6,0) zigzag single-walled boron phosphide nanotubes: A computational study. *Comput. Theor. Chem.* **2011**, *972*, 14–19. [CrossRef]

20. Rezaei-Sameti, M. Gallium doped in armchair and zigzag models of boron phosphide nanotubes (BPNTs): A NMR study. *Phys. B Condens. Matter* **2012**, *407*, 3717–3721. [CrossRef]

21. Baei, M.T.; Peyghan, A.A.; Moghimi, M. Electronic structure study of Si-doped (4,4) armchair single-walled boron phosphide nanotube as a semiconductor. *Monatsh. Chem.* **2012**, *143*, 1627–1635. [CrossRef]

22. Baei, M.T.; Sayyad-Alangi, S.Z.; Moradi, A.V.; Torabi, P. NMR and NQR parameters of the SiC-doped on the (4,4) armchair single-walled BPNT: A computational study. *J. Mol. Model.* **2011**, *18*, 881–889. [CrossRef] [PubMed]

23. Baei, M.T. Ge-doped (4,4) armchair single-walles boron phosphide nanotube as a semiconductor: A computational study. *Monatsh. Chem.* **2012**, *6*, 881–889. [CrossRef]

24. Srivastava, A.; Sharma, M.; Tyagi, N.; Kothari, S.L. Diameter Dependent Electronic Properties of Zigzag Single Wall BX (X = N, P, As) Nanotubes: Ab-Initio Study. *J. Comput. Theor. Nanosci.* **2012**, *9*, 1693–1699. [CrossRef]

25. Salabat, K.; Azizi, K. A Computational Study on the Effects of Size and Chirality on the Electronic and Structural Properties of BP Nanotubes. In Proceedings of the 16th Iranian Physical Chemistry Conference, Mazandaran, Iran, 29–31 October 2013; Volume 16, pp. 867–869. Available online: https://www.sid.ir/FileServer/SE/247E20131694.pdf (accessed on 9 May 2021).

26. Frish, M.J.; Trucks, G.W.; Schlegel, H.B.; Scuseria, G.E.; Robb, M.A.; Cheeseman, J.R.; Montgomery, J.A., Jr.; Vreven, T.; Kudin, K.N.; Burant, J.C.; et al. *G09W*®; Gaussian, Inc.: Wallingford, CT, USA, 2016.

27. Hou, N.; Wu, Y.Y.; Wei, Q.; Liu, X.L.; Ma, X.J.; Zhang, M.; Wu, H.S. A comparative theoretical study on the electrical and nonlinear optical properties of Li atom adsorbed on AlN and BN single-walled nanotubes. *J. Mol. Model.* **2017**, *23*, 1–8. [CrossRef] [PubMed]

28. Mardirossian, N.; Head-Gordon, M. How Accurate Are the Minnesota Density Functionals for Noncovalent Interactions, Isomerization Energies, Thermochemistry, and Barrier Heights Involving Molecules Composed of Main-Group Elements? *J. Chem. Theory Comput.* **2016**, *12*, 4303–4325. [CrossRef] [PubMed]

29. Zhao, Y.; Truhlar, D.G. The M06 suite of density functionals for main group thermochemistry, thermochemical kinetics, noncovalent interactions, excited states, and transition elements: Two new functionals and systematic testing of four M06-class functionals and 12 other functionals. *Theor. Chem. Acc.* **2007**, *120*, 215–241.

30. Koopmans, T. Über die Zuordnung von Wellenfunktionen und Eigenwerten zu den Einzelnen Elektronen Eines Atoms. *Physica* **1934**, *1*, 104–113. [CrossRef]

31. Parr, R.G.; Pearson, R.G. Absolute hardness: Companion parameter to absolute electronegativity. *J. Am. Chem. Soc.* **1983**, *105*, 7512–7516. [CrossRef]

32. Parr, R.G.; Szentpály, L.v.; Liu, S. Electrophilicity Index. *J. Am. Chem. Soc.* **1999**, *121*, 1922–1924. [CrossRef]

33. Juárez, A.R.; Anota, E.C.; Cocoletzi, H.H.; Ramírez, J.S.; Castro, M. Stability and electronic properties of armchair boron nitride/carbon nanotubes. *Fuller. Nanotub. Carbon Nanostruct.* **2017**, *25*, 716–725. [CrossRef]

34. Beheshtian, J.; Soleymanabadi, H.; Kamfiroozi, M.; Ahmadi, A. The H2 dissociation on the BN, AlN, BP and AlP nanotubes: A comparative study. *J. Mol. Model.* **2011**, *18*, 2343–2348. [CrossRef] [PubMed]

35. Mirzaei, M.; Giahi, M. Computational studies on boron nitride and boron phosphide nanotubes: Density functional calculations of boron-11 electric field gradient tensors. *Phys. E Low Dimens. Syst. Nanostruc.* **2010**, *42*, 1667–1669. [CrossRef]

36. Arshadi, S.; Bekhradnia, A.R.; Alipour, F.; Abedini, S. Pure and carbon-doped boron phosphide (6,0) zigzag nanotube: A computational NMR study. *Phys. B Condens. Matter* **2015**, *477*, 1–7. [CrossRef]

37. Rezaei-Sameti, M.; Yaghoobi, S. Theoretical study of adsorption of CO gas on pristine and AsGa-doped (4, 4) armchair models of BPNTs. *Comput. Condens. Matter* **2015**, *3*, 21–29. [CrossRef]

38. Geerlings, P.; De Proft, F.; Langenaeker, W. Conceptual Density Functional Theory. *Chem. Rev.* **2003**, *103*, 1793–1874. [CrossRef]

39. Parr, R.G. Density Functional Theory of Atoms and Molecules. *Horiz. Quantum Chem.* **1980**, *3*, 5–15.

40. Chermette, H. Chemical reactivity indexes in density functional theory. *J. Comput. Chem.* **1999**, *20*, 129–154. [CrossRef]
41. Roos, G.; Geerlings, P.; Messens, J. Enzymatic Catalysis: The Emerging Role of Conceptual Density Functional Theory. *J. Phys. Chem. B* **2009**, *113*, 13465–13475. [CrossRef]
42. Hosseinzadeh, B.; Salimi Beni, A.; Eskandari, R.; Karami, M.; Khorram, M. Interaction of propylthiouracil, an anti-thyroid drug with boron nitride nanotube: A DFT study. *Adsorption* **2020**, *26*, 1385–1396. [CrossRef]
43. Makiabadi, B.; Zakarianezhad, M.; Hosseini, S.S. Investigation and comparison of pristine/doped BN, AlN, and CN nanotubes as drug delivery systems for Tegafur drug: A theoretical study. *Struct. Chem.* **2021**, *32*, 1019–1037. [CrossRef]
44. Chen, K.; Zeng, Q.; He, G.; Sarkar, A. Tyrosine amino acid as a sustainable material for chemical functionalization of single-wall BC2N nanotubes: Quantum chemical study. *Struct. Chem.* **2021**, *32*, 1197–1203. [CrossRef]
45. Muz, İ.; Kurban, H.; Kurban, M. A DFT study on stability and electronic structure of AlN nanotubes. *Mater. Today Commun.* **2021**, *26*, 102118. [CrossRef]
46. García-Toral, D.; Báez, R.M.; Sánchez, S.J.I.; Flores-Riveros, A.; Cocoletzi, G.H.; Rivas-Silva, J.F. Encapsulation of Pollutant Gaseous Molecules by Adsorption on Boron Nitride Nanotubes: A Quantum Chemistry Study. *ACS Omega* **2021**, *6*, 14824–14837. [CrossRef] [PubMed]
47. Beheshtian, J.; Peyghan, A.A.; Bagheri, Z. Carbon nanotube functionalization with carboxylic derivatives: A DFT study. *J. Mol. Model.* **2013**, *19*, 391–396. [CrossRef]
48. Chermahini, A.N.; Teimouri, A.; Farrokhpour, H. A DFT-D study on the interaction between lactic acid and single-wall carbon nanotubes. *RSC Adv.* **2015**, *5*, 97724–97733. [CrossRef]
49. Mendoza-Wilson, A.M.; Glossman-Mitnik, D. CHIH-DFT study of the electronic properties and chemical reactivity of quercetin. *J. Mol. Struct. THEOCHEM* **2005**, *716*, 67–72. [CrossRef]
50. Erkoç, Ş.; Malcioğlu, O.B.; Taşci, E. Structural and electronic properties of single-wall GaN nanotubes: Semi-empirical SCF-MO calculations. *J. Mol. Struct. THEOCHEM* **2004**, *674*, 1–5. [CrossRef]
51. Kaur, J.; Singla, P.; Goel, N. Adsorption of oxazole and isoxazole on BNNT surface: A DFT study. *Appl. Surf. Sci.* **2015**, *328*, 632–640. [CrossRef]
52. Sánchez, S.J.I.; Rivas-Silva, J.F.; García-Toral, D. Study of weak interactions of boron nitride nanotubes with anticancer drug by quantum chemical calculations. *Theor. Chem. Acc.* **2020**, *139*, 1–9. [CrossRef]
53. Makiabadi, B.; Zakarianezhad, M.; Nasab, S.S. Theoretical study of interaction of NH_2X (X = H, CH_3, CH_2OCH_3, and CH_2COOH) molecules with AlN and AlP nanotubes. *Phosphorus Sulfur Silicon Relat. Elem.* **2017**, *192*, 81–87. [CrossRef]
54. Mananghaya, M.R.; Santos, G.N.; Yu, D.N. Solubility of amide functionalized single wall carbon nanotubes: A quantum mechanical study. *J. Mol. Liq.* **2017**, *242*, 1208–1214. [CrossRef]
55. Beheshtian, J.; Peyghan, A.A.; Tabar, M.B.; Bagheri, Z. DFT study on the functionalization of a BN nanotube with sulfamide. *Appl. Surf. Sci.* **2013**, *266*, 182–187. [CrossRef]
56. Mananghaya, M. Modeling of single-walled carbon nanotubes functionalized with carboxylic and amide groups towards its solubilization in water. *J. Mol. Liq.* **2015**, *212*, 592–596. [CrossRef]